



HAL
open science

Effect of thermal-treatment on structural, mössbauer and magnetic properties of ZN-Nanoferrite

Shashank Kane, Roshni Verma, Salil Modak, Varimalla Raghavendra Reddy,
Frédéric Mazaleyrat

► **To cite this version:**

Shashank Kane, Roshni Verma, Salil Modak, Varimalla Raghavendra Reddy, Frédéric Mazaleyrat. Effect of thermal-treatment on structural, mössbauer and magnetic properties of ZN-Nanoferrite. ICAME 2023, Sep 2023, Carthagène des Indes, Colombia. pp.36, 10.1007/s10751-024-01881-6 . hal-04501768

HAL Id: hal-04501768

<https://hal.science/hal-04501768>

Submitted on 12 Mar 2024

HAL is a multi-disciplinary open access archive for the deposit and dissemination of scientific research documents, whether they are published or not. The documents may come from teaching and research institutions in France or abroad, or from public or private research centers.

L'archive ouverte pluridisciplinaire **HAL**, est destinée au dépôt et à la diffusion de documents scientifiques de niveau recherche, publiés ou non, émanant des établissements d'enseignement et de recherche français ou étrangers, des laboratoires publics ou privés.



Distributed under a Creative Commons Attribution 4.0 International License

EFFECT OF THERMAL-TREATMENT ON STRUCTURAL, MÖSSBAUER AND MAGNETIC PROPERTIES OF ZN-NANOFERRITE

S. N. Kane^{1,*}, R. Verma¹, S. S. Modak¹, V. R. Reddy², and F. Mazaleyrat³

¹Magnetic Materials Laboratory, School of Physics, D. A. University, Indore-452001, India

²UGC-DAE Consortium for Scientific Research, University Campus, Khandwa Road, Indore-452001, India

³SATIE, ENS Paris-Saclay, 4 Avenue des Sciences, 91190 Gif-sur-Yvette, France

Abstract

We report synthesis of spinel ZnFe_2O_4 ferrite by solution combustion method. Room temperature x-ray diffraction 'XRD'; magnetic; ^{57}Fe Mössbauer measurements were used to probe thermal treatment dependence of the structural, magnetic properties, and connection between them. Mössbauer spectroscopy was particularly used to identify the presence of magnetic/non-magnetic phases, their effect on magnetic properties. XRD confirms the formation of spinel phase, trace of $\alpha\text{-Fe}_2\text{O}_3$ was also detected. Thermally treated samples show: i) substantial increase of grain diameter: 20.3 to 48.8 nm, presence of compressive-strain, ii) increase of inversion parameter: 0.20 to 0.65, iii) redistribution of Zn^{2+} , Fe^{3+} ions on A, B site, therefore increasing the disorder, iv) strengthening of A-O-B, A-O-A, with simultaneous weakening of B-O-B superexchange interaction, v) increase of magnetic-dead-layer thickness, thus affecting magnetic properties. Coercivity variation with grain diameter suggests that the studied samples lie in the overlap region between single/multiple-domains. Non-zero canting angle suggests the applicability of Yafet-Kittel three sub lattice model. Magnetization behaviour is explained using core (ordered-spin)-shell (spin-canting) model. Mössbauer results confirm: a) the 3+ state of Fe ions, b) the presence of $\alpha\text{-Fe}_2\text{O}_3$ phase, and being antiferromagnetic reduces the saturation magnetization. Thermal treatment assisted modification of line width range between 0.42 to 0.72 mm/s, is attributable to surface strain/domain pinning. Mössbauer spectra confirm the presence of two superparamagnetic doublets that are explained by core (lower quadrupole splitting) - shell (higher quadrupole splitting) model. XRD, magnetic measurements combined with Mössbauer spectroscopy, provide improved understanding on the effect of thermal treatments on magnetic properties.

Keywords: Zn-ferrite, Mössbauer spectroscopy, spark plasma sintering, cationic distribution, magnetic properties

*Corresponding author, e mail: kane_sn@yahoo.com

1. Introduction

Spinel ferrites have face centred cubic lattice, defined by $(M^{2+}) [Fe^{3+}]_2O_4$, with two inter-penetrating sub-lattices: tetrahedral site (A), octahedral site [B], where structural, and magnetic properties are different. Literature shows that synthesis protocol e. g. - [1–4], presence of specific cations, post-preparation thermal treatment [5 – 6], distributions of cations on A, B sites [1 – 2] play a key role in determining their structural, and magnetic properties of spinel ferrites e. g. – Zn ferrite. Thus, making them interesting for various applications, including those in magnetic cores, gas sensing, multilayer chip inductor, high frequency devices, biomedical applications: magnetic hyperthermia for cancer treatment, enhanced MRI imaging etc. [7]. Zn ferrite is of interest, not only from basic research point of view, nonetheless it shows excellent chemical stability, mechanical hardness, low coercivity, moderate saturation magnetization, making it a good candidate as soft magnetic, low-loss material at higher frequencies [6]. In bulk form $ZnFe_2O_4$ has normal spinel structure where Zn^{2+} ions occupy A-site, Fe^{3+} ions reside on B-site, described by formula: $(Zn^{2+})[Fe^{3+}]O_4$, where () and [] brackets represent respectively A, B sites. However, $ZnFe_2O_4$ in nanocrystalline form shows mixed spinel ferrites that are described by $(Zn^{2+}_{1-\delta}Fe^{3+}_{\delta})[Zn^{2+}_{\delta}Fe^{3+}_{2-\delta}]O_4$, (δ : inversion parameter), with both A, B sites occupied by Zn^{2+} , Fe^{3+} ions. Published works show that in case of nanocrystalline $ZnFe_2O_4$ cationic-redistribution can be achieved by thermal treatments e. g. - [8 – 9], would reflect in magnetic properties [3, 6, 8], ascribable to stronger inter-sub-lattice A–O–B super-exchange interaction, in comparison to intra-sub-lattice A–O–A, B–O–B interactions. Numerous literature e. g. - [1-13] report structural, and magnetic properties of $ZnFe_2O_4$ probed via complementary experimental techniques: x-ray diffraction ‘XRD’; magnetic measurements, Mössbauer measurements, neutron diffraction etc. Nevertheless, a comparison of structural, and magnetic properties among various $ZnFe_2O_4$ samples: i) without any thermal treatment, ii) conventional thermal treatment, and iii) spark plasma sintered ‘SPS’ is less-explored, and would provide vital information on thermal treatment induced structural changes, evolution of magnetic and/or non-magnetic phase, and its effect on magnetic properties.

Thus, we report solution combustion synthesis of $ZnFe_2O_4$, using nitrate-citrate precursors. Room temperature x-ray diffraction (XRD); magnetic measurements, ^{57}Fe Mössbauer measurements were used to probe the thermal-treatment (*conventional thermal treatment*, SPS) dependency of properties of Zn-ferrite and correlation between them. Mössbauer spectroscopy was particularly used to identify the presence of magnetic / non-magnetic phase, and its effect on magnetic properties.

2. Experimental details

2.1 Material synthesis and thermal treatment

Solution combustion method utilizing AR grade Zinc nitrate: $Zn(NO_3)_2 \cdot 6H_2O$, Ferric Nitrate: $Fe(NO_3)_3 \cdot 9H_2O$, and Citric acid: $C_6H_8O_7$, were used in stoichiometric ratio, keeping metal salt to citric acid ratio as 1:1, were used to prepare $ZnFe_2O_4$. Precursors were mixed in deionized water, and pH was maintained at 7 by adding Ammonia solution: NH_4OH , and solution was heated at ~ 115 °C in air till soft powder (called as dry gel) is formed. Synthesized ‘dry gel’ (labelled as DG) sample was annealed at 600 °C / for 3 hours (labelled as ANN), and was also spark plasma sintered at 800 °C for 5 minutes (labelled as SPS). It is of value to note that Spark Plasma Sintering (SPS) is a sintering technique which involves the simultaneous usage of uniaxial pressure, and high-intensity pulsed current (low-voltage) flowing directly through the sample leads to heating. So SPS can be treated as a variation of hot-pressing, and here the furnace is substituted by a cast which contains the sample. Distinct advantages of SPS include: fast (\sim few minutes), and uniform sintering, high

heating rate (heating rate ~ 1000 °C /min), relatively low grain growth etc. [14], thus can be effectively used for preparing nano-crystalline materials. Samples were *Spark Plasma Sintered* in Sumitomo Dr. Sinter 515 S SYNTEX spark plasma sintering machine under Argon atmosphere. Samples were filled in an 8 mm graphite die with a layer of protective graphite foil, and closed on both sides by Carbon pistons, and a uniaxial pressure of 50 MPa was applied. Within 8 min., the sample temperature was raised up to 800 °C, measured by a thermocouple located inside the die. This temperature was kept for a duration of 5 minutes, and then the sample was cooled within 8 min. Heating / cooling rate was 100 K / min. Figure 1 (a to c) respectively depicts the schematic of sample synthesis-thermal annealing, schematic of SPS apparatus, and temperature profile of SPS process.

2.2 Material characterization

X-ray diffraction measurements (Bruker D8 Advance diffractometer employing $\text{CuK}\alpha$ radiation, wavelength: 0.15418 nm) were done at room temperature. Transmission ^{57}Fe Mössbauer spectra were recorded at room temperature in constant acceleration mode using $^{57}\text{Co}:\text{Rh}$ source by using standard PC-based Mössbauer spectrometer utilizing Wissel velocity drive. Natural iron absorber at room temperature was used for the velocity calibration. Lakeshore Model 7410 vibrating sample magnetometer ($H_{\text{max}} = \pm 1.9$ T) operating at room temperature was used to obtain hysteresis loops.

2.3 Analysis of the data

XRD data analysis gives a_{exp} , and (311) reflection was used for a_{exp} calculation. Grain diameter $D_{\text{W-H}}$, strain ϵ , is computed by Williamson-Hall (W-H) analysis. Dislocation density was computed by following expression: $\rho_{\text{D}} = 15\epsilon / a_{\text{exp}} \times D_{\text{W-H}}$ (lines/m²), where ϵ : strain, a_{exp} : Experimental lattice parameter, $D_{\text{W-H}}$: Grain diameter. Distribution of cations on A, B site was calculated by using Bertaut method [15], by comparing the ratios of experimental, computed intensity for: (422), (311), (400), (220) planes [16]. Distribution of cations on A and B site, where theoretical, and experimental ratios ($I_{\text{hkl}}^{\text{obs}}$ and $I_{\text{hkl}}^{\text{cal}}$) of the observed, calculated intensities agree noticeably, is taken as correct one [17]. Neel magnetic moment i. e. theoretical magnetization at 0 K: ' $M_{\text{s(th)}}$ ', theoretical lattice parameter (a_{th}), bond angles ($\theta_1, \theta_2, \theta_3, \theta_4, \theta_5$), Oxygen position parameter (u), and inversion parameter (δ) were also computed from cationic distribution, as detailed in [17]. A MATLAB[®] program was written for calculating a_{th} , u , $\theta_1, \theta_2, \theta_3, \theta_4, \theta_5, M_{\text{s(th)}}$, utilizing the expressions, which are given in Supplementary Materials. NORMOS SITE program [18] was used for computer fitting of Mössbauer spectra, assuming Lorentzian line shapes, and resolved into two sub-spectra, to obtain hyperfine parameters. Hysteresis loops were used to get saturation magnetization (M_{s}), coercivity (H_{c}), and squareness ratio ($M_{\text{r}}/M_{\text{s}}$). Anisotropy constant K_1 was calculated by using the equation: $K_1 = (H_{\text{c}} \times M_{\text{s}}) / 0.96$, where M_{s} : saturation magnetization, H_{c} : coercivity. As hysteresis loops are not saturated, the saturation magnetization ' M_{s} ' values were obtained by plotting magnetization ' M ' versus $1/H$ (magnetic field), and a linear fit was obtained with extrapolation to zero, where curve intersects the y-axis, is taken as saturation magnetization ' M_{s} ' [19]. Canting angle $\alpha_{\text{Y-K}}$ was computed as detailed in [20], and the expression for $\alpha_{\text{Y-K}}$ is given in Supplementary Materials. Magnetic dead layer thickness (t) was calculated as described in [19, 21-22] and the expression for t is given in Supplementary Materials. Error shown in tables, figures is Standard Deviation obtained from the data.

3. Results and discussion

Figure 2 depicts the XRD patterns of the studied samples, confirming the formation of nanocrystalline spinel phase (grain diameter range between 20.3 to 48.6 nm), and shows presence of strong diffraction peaks corresponding to

(220), (311), (222), (400), (422), (511), (440) planes. Rietveld refined XRD patterns, and Rietveld refined R-parameters (R_{wp})

R_p , R_{exp}), goodness of fit ($GOF = R_{wp}/R_{exp}$), and the shape parameters (u , v , w) are given respectively as figure S1, and table S1 in Supplementary Materials. In ANN sample, presence of α -Fe₂O₃ (~ 2 %) was also reported in [6, 10], ascribable to moderate thermal annealing temperature (600 °C) [23], and antiferromagnetic nature of α -Fe₂O₃ is expected to reduce the saturation magnetization ($M_{s(exp)}$) of the ANN sample. Table 1 gives lattice parameter (a_{exp}), Williamson-Hall grain diameter (D_{W-H}), strain (ϵ), dislocation density (ρ_D) for the studied DG, ANN, SPS samples. Thermal treatment induced increase of a_{exp} . given as inset of fig. 2 for ANN, SPS samples, showing the expansion of unit cell, and is consistent with earlier results [5, 23]. Perusal of table 1 shows that thermal treatment leads to increase of Williamson-Hall grain diameter (D_{W-H}) from 20.3 to 48.6 nm that is consistent with earlier reports [6, 24]. Negative sign of strain (W-H plot with negative slope) in the studied samples reveal compressive strain, and is attributable to thermal treatment induced structural changes, as were also reported in [25], and would have effect on magnetic properties [26]. Thermal treatment also leads to variation of dislocation density (ρ_D), and would mirror in magnetic properties, as was also reported in [26].

Table 2 depicts calculated distribution of Zn²⁺, Fe³⁺ cations on A, B site, a_{exp} , a_{th} , Oxygen parameter u and Calc., Obs. intensity ratios: I_{220}/I_{440} , I_{400}/I_{422} , I_{220}/I_{440} . Perusal of table 2 shows that as we move from DG to ANN sample, on B-site: there is reduction of population of Fe³⁺ ions (*migration of Fe³⁺ ions from B to A site*) with concurrent increase of Zn²⁺ ions (*migration of Zn²⁺ ions from A to B site*). As we move from ANN sample to SPS sample, there is further migration of Fe³⁺ ions from A to B site, while Zn²⁺ ions migrate from B to A site. Observed modification of cationic distribution is ascribable to thermal annealing assisted movement of Fe³⁺, Zn²⁺ cations on A, B site [27]. Table 2 also shows good matching of a_{exp} , a_{th} , and Obs. Calc. intensity ratios- I_{220}/I_{440} , I_{400}/I_{422} , I_{220}/I_{440} , validating the reliability of the obtained distribution of Zn²⁺, Fe³⁺ cations on A, B site. Observed changes in cationic distribution leads to variation of strain in the studied DG, ANN, SPS samples, as shown in table 1. It is worth noting that ionic radius of Fe³⁺ is 0.067 nm, and that of Zn²⁺ is 0.074 nm. So the variation of population of Fe³⁺, Zn²⁺ on A, B sites would lead to alteration of a_{exp} in the studied DG, ANN, SPS samples [28]. Variation of cationic distribution in DG, ANN, SPS samples leads to alteration of inversion parameter (δ) [27], ranging between 0.2 to 0.65, and Oxygen positional parameter (u) ranging between 0.3807 to 0.3845, which is higher than ideal spinel structure (0.375) [29], indicates increased disorder [19, 26]. In an ideal spinel ferrite, oxygen ions form an fcc lattice with cubic edge as: $0.5 a_{exp}$. and Oxygen positional parameter (u) is 0.375, which is valid for an ideal case, but considering an actual spinel ferrite, the A-site (tetrahedral-site) is somewhat small to accommodate a metal ion causing minor lattice distortions, and there would be a movement of the four oxygen atoms, as is observed by changes in a_{exp} . shown as inset of fig. 2. So in the studied samples, obtained higher u can be utilized for approximate measurement of oxygen movement. In the studied DG, ANN, SPS samples, obtained higher u values are ascribable to different concentration of Zn²⁺ ions on A-site (see table 2). So, more the concentration of Zn²⁺ ions on A-site, larger will be the displacement of oxygen anions. This declaration is confirmed in figure 3 showing linear variation of u with δ [17, 20], described by experimental relation: $u = 0.39 - 0.0083 (\delta)$. Obtained variation of Oxygen positional parameter is expected to affect the magnetic properties [26].

Figure 4 gives the variation of bond angles for the studied, DG, ANN, SPS samples. Bond angles θ_1 , θ_2 reveal information on A-O-B, while θ_3 , θ_4 provide information on B-O-B, and θ_5 gives information on A-O-A super-exchange interaction [26, 29]. Perusal of fig. 4 reveal that as we go from DG → SPS → ANN samples, increase of θ_1 , θ_2 , θ_5 with simultaneous decrease of θ_3 , θ_4 indicate respectively the strengthening of A-O-B, A-O-A interaction, and weakening of B-O-B interaction, and would reveal changes in magnetic properties, which is consistent with earlier studies [17, 19, 28].

Figure 5 shows Hysteresis loops of the studied DG, ANN, SPS samples, whereas inset shows linear increase of $M_{s(\text{exp.})}$ dependence with Oxygen parameter u , described by fitting equation: $M_{s(\text{exp.})} = 1148.56 (u) - 432.05$, ascribable to increased disorder in the studied specimens [19, 22, 30]. The un-saturated hysteresis loops of DG, ANN, SPS samples

shown in figure 5 are typical of superparamagnetic **behaviour** with negligibly small remanence (M_r), and moderate coercivity (H_c).

Table 3 depicts the dependence of magnetic parameters: experimental ($M_{s(\text{exp.})}$); theoretical saturation magnetization ($M_{s(\text{th.})}$), coercivity (H_c), remanence (M_r), squareness ratio (M_r/M_s), magnetocrystalline anisotropy (K_1), canting angle (α_{Y-K}), and dead layer thickness (t). In the framework of Stoner–Wohlfarth (SW) model [31] for three-dimensional non-interacting random particles, $M_r/M_s \sim 0.5$ represents randomly oriented uniaxial anisotropic ferromagnetic particles. Perusal of table 3 shows that for the studied DG, ANN, SPS samples, M_r/M_s values range between 0.0014 to 0.0678, which is far lower than 0.5, are ascribable to much stronger interactions among multi-domain grains [32]. Therefore, SW model would be less relevant for the studied samples and hence, using M_r/M_s values it cannot be said evidently, that the studied samples possess uniaxial anisotropy, as was also reported in [30].

Figure 6 (a, b) shows the variation of $M_{s(\text{th.})}$, $M_{s(\text{exp.})}$ for DG, ANN, SPS samples, and the non-similar trend of $M_{s(\text{th.})}$, $M_{s(\text{exp.})}$, finite α_{Y-K} values (see table 3) shows that the magnetization **behaviour** is governed by Yafet–Kittel (Y–K) three sub lattice model [33, 34]. Fig. 6 (c) shows decrease of $M_{s(\text{exp.})}$ with increase of dead layer thickness ' t ', ascribed to higher spin disorder at the surface ('shell') of the nanoparticles, and will decrease the saturation magnetization [17, 19, 22, 35]. Fig 6 (c) inset shows variation of $M_{s(\text{exp.})}$ with D_{W-H} , and as D_{W-H} increases from 20.3 nm (*DG sample*) to 48.6 nm (*SPS sample*), $M_{s(\text{exp.})}$ drops from 10.17 Am²/kg to 7.35 Am²/kg **showing** that with increasing grain diameter (D_{W-H}), $M_{s(\text{exp.})}$ decreases, is consistent earlier study [1], ascribable to thermal treatment assisted variation of inversion degree. In addition, for smaller grain diameter, surface effects become progressively important due to higher surface to volume ratio, generating higher strain on surface (as seen in table 1), would also have effect on the magnetization. Figure 6 (d), illustrates the pictorial representation of core–shell structure of nanoferrite, where ferrite nano particles are considered as: i) inner core with spin arrangement, parallel to applied magnetic field, and ii) surface layer with spins inclined and/or their canting at some angle (and not at random) with respect to the applied magnetic field direction due to the presence of vacancies in nanoparticles, however the chances of spin canting in the core cannot be ruled out [35]. Figure 6 (e) depicts the linear increase of H_c with K_1 , and is consistent with earlier reports [17, 19], represented by experimental relation: $H_c = 28.12 K_1 - 3.13$. Dependence of H_c with D_{W-H} (see fig. 6 e), suggests that the studied samples lie in the overlap region between multiple-domains/single-domain [17, 19, 26, 36]. It is worth mentioning that SPS sample displays better soft magnetic properties: low H_c , moderate M_s , low K_1 as compared to DG, ANN samples, exhibits the utility of 'spark plasma sintering' to obtain soft magnetic properties in ZnFe₂O₄.

Figure 7 **shows** Mössbauer spectra **and** table 4 **lists their corresponding fitted hyperfine interaction**. **Fitted** isomer shift for all the studied samples (see table 4) **reveal** that Fe has 3+ oxidation state, and is consistent with literature [17, 26, 37]. In the studied DG, ANN, SPS samples, thermal treatment assisted modification of line-width range between 0.42 to 0.72 mm/s is attributable to surface strain or domain pinning [38-39]. Mössbauer spectrum of ANN sample is best fitted with two components: i) a sextet linked to surface 'shell' [40] ascribable to α -Fe₂O₃ (*as was also detected in XRD data, shown in fig. 2*) with IS = 0.38 mm/s, QS = - 0.2 mm/s, and $B_{\text{hf}} = 52.5$ Tesla, which closely match with earlier works [41-42], **has** 21% area, and ii) a superparamagnetic doublet, and in the framework of core-shell model [35, 40, 43-46] is connected with inner 'core' with IS = 0.34 mm/s, QS = 0.38 mm/s and area of 79 %, ascribable to superparamagnetic spinel phase [42]. Mössbauer spectra of DG, SPS samples are best fitted with two doublets, and core-shell model can be used to describe these two doublets [35, 40, 43 – 46] and are linked **respectively** to Fe³⁺ ions

from 'core' and 'shell' (surface and/or interface) of the ferrite nanoparticles (see fig. 6 d). As shown in table 4, doublet

1 with lower QS is associated with nanoparticle ‘core’, and the doublet 2 with higher QS is connected to ‘shell’ (interface) of Fe³⁺ ions. It is worth noting that, in case of nanoparticles, large surface to volume ratio leads to change in spherically symmetric charge distribution, thus creating an electric field gradient [45]. Consequently, there is modification of QS corresponding to doublet 2. Doublet 1 in DG sample is connected with inner ‘core’ with IS = 0.33 mm/s, QS = 0.41 mm/s, and area = 53 %, while doublet 2 is associated with ‘shell’ (interface) with IS = 0.33 mm/s, QS = 0.96 mm/s, and area = 47 %. In SPS sample, doublet 1 is related to inner ‘core’ with IS = 0.35 mm/s, QS = 0.25 mm/s, and area = 62 %, whereas doublet 2 is linked to ‘shell’ (interface) with IS = 0.32, QS = 0.65 mm/s, area = 38 %. It is worth mentioning here that in the studied DG, ANN, SPS samples, thermal-treatment assisted evolution of magnetic properties (saturation magnetization, coercivity etc.) is a combined effect of the modification of: grain diameter, cationic distribution, oxygen positional parameter, strain, canting angle, dead layer thickness, as-well-as the presence of doublet and/or sextet: α -Fe₂O₃, (detectable via Mössbauer measurements). Thus, complementary experimental techniques: XRD, magnetic measurements combined with Mössbauer spectroscopy, contribute decisively in improved understanding of the effect of thermal treatments on the magnetic properties of spinel ZnFe₂O₄ nanoferrites.

Summary

Formation of nanocrystalline spinel Zn-ferrite phase, and presence of minor α -Fe₂O₃ phase is confirmed by XRD. Thermal treatment is accountable for the observed increase of W-H grain diameter: range between 20.3 to 48.6 nm, and lowering of compressive strain, dislocation density. In the studied DG, ANN, SPS samples, redistribution of Zn²⁺, Fe³⁺ ions on A, B site is observed, although both Zn²⁺, Fe³⁺ ions are present on A, B site. Observed cationic redistribution is responsible for increase of disorder, degree of inversion, modification of canting angle, increase of magnetic dead layer thickness, and also the increase of a_{exp} . As we go from DG → SPS → ANN sample, alteration of bond angles (θ_1 to θ_5) leads to weakening of B–O–B superexchange interaction with synchronized strengthening of A–O–B, A–O–A superexchange interaction. These structural changes mirror in magnetic properties, showing alteration of coercivity, saturation magnetization, and are understood in the framework of Y–K three-sub-lattice model. Hysteresis loops of DG, ANN, SPS samples show superparamagnetic behaviour with negligibly small remanence (M_r) and moderate coercivity (H_c). Magnetic properties are understood by using core (ordered spin)–shell (canted spin) model. Increase of Mössbauer linewidth suggests the variation of surface strain, domain pinning, leading to the variation of both coercivity, and saturation magnetization. Presence of two superparamagnetic doublets in Mössbauer spectra are explained by core–shell model. Present studies offer better understanding of the thermal treatments induced structural changes, and its effect on magnetic properties of the studied DG, ANN, SPS samples. SPS sample shows better soft magnetic properties (low H_c , moderate M_s , and low anisotropy) as compared to DG, ANN samples, demonstrating the effectiveness of ‘spark plasma sintering’ technique to achieve soft magnetic properties in ZnFe₂O₄.

Acknowledgements:

Authors thank Dr. M. Gupta UGC-DAE CSR, Indore, for XRD measurements. SNK acknowledges gratefully for one month “Invited Professor” stay at ENS Paris-Saclay, Cachan (France). Work supported by DAVV Seed money grant No. Dev / Seedmoney 2.0 / 2020-21 / 649, 20 Jan. 2022.

Author contributions:

S. N. Kane: Conception, design, Supervision, Resources, preparation of samples, sample characterization, data analysis, writing manuscript.

R. Verma: Structural data analysis, manuscript writing.

S. S. Modak: XRD data analysis, manuscript writing.

V. R. Reddy: Mössbauer characterization, data analysis, writing manuscript.

F. Mazaleyrat: Magnetic measurements, data analysis, manuscript writing.

Funding Work supported by DAVV Seed money grant No. Dev/Seedmoney2.0/2020-21/649, 20 Jan. 2022.

Data availability The data that support the findings of this work are available from the corresponding author, upon reasonable request.

Declarations:

Ethical approval Not applicable.

Consent to participate All authors voluntarily agree to participate in this study.

Consent for publication All the authors have read, agreed to give their consent for publication of the current version of the submitted manuscript.

Competing interests The authors declare no competing interests.

References:

- [1] Atif, M, Hasanain, S. K., M. Nadeem, M: Magnetization of sol–gel prepared zinc ferrite nanoparticles: Effects of inversion and particle size, *Solid State Comm.* **138**, (2006) 416–421.
- [2] Jiang, J. Z., Wynn, P., S. Morup, S., Okada, T., Berry, F. J.: Magnetic structure evolution in mechanically milled nanostructured ZnFe_2O_4 particles. *Nanostruct. Mater.* **12**, 737–740 (1999).
- [3] S.D. Shenoy, S. D., Joy, P. A., Anantharaman, M. R.: Effect of mechanical milling on the structural, magnetic and dielectric properties of coprecipitated ultrafine zinc ferrite. *J. Magn. Magn. Mater.* **269**, 217–226 (2004).
- [4] Yu, S. H., Fujino, T., Yoshimura, M.: Hydrothermal synthesis of ZnFe_2O_4 ultrafine particles with high magnetization. *J. Magn. Magn. Mater.* **256**, 420–424 (2003).
- [5] Tanaka, K., Makita, M., Soga, N. L: Effect of Heat Treatment on Magnetic Properties of Ferrimagnetic Zinc Ferrite Prepared by Rapidly Quenching Method. *J. Magn. Soc. of Japan* **22(S1)**, 77-79 (1998)
- [6] Naseri, M. G. Saion, E. B., Hashima, M. , Shaari, A. H. , Ahangar, H. A. : Synthesis and characterization of zinc ferrite nanoparticles by a thermal treatment method. *Solid State Comm.* **151**, 1031 – 1035 (2011)
- [7] Willard, M.A., Kurihara, L.K., Carpenter, E.E., Calvin, S., Harris, V.G.: Chemically prepared magnetic nanoparticles. *Int. Mater. Rev.* **49**, 125–170 (2004)
- [8] Hamdeh, H.H., Ho, J.C., Oliver, S.A., Willey, R.J., Oliver, G., Busca, G.: Magnetic properties of partially inverted Zinc ferrite aerogel powder. *J. Appl. Phys.* **81(4)**, 1851–1857 (1997)
- [9] Kamiyama, T., Haneda, K., Sato, T., Ikeda, S., Asano, H.: Cation distribution in ZnFe_2O_4 fine particles studied by neutron powder diffraction. *Solid State Commun.* **81**, 563–566 (1992)
- [10] Mahmoud, M., Hassan, A. M., Mamdouh Abdel aal Ahmed, M. A. aal, Zhu, K. Ganeshraja, A. S., Wang, J.: Mössbauer and magnetic studies of nanocrystalline zinc ferrites synthesized by microwave combustion method, *Hyperfine Inter.* **237**, 17-1 – 17-11 (2016)
- [11] Choi, E. J., Ahn, Y, Song, Ki-Chang: Mössbauer study in zinc ferrite nanoparticles. *J. Magn. Magn. Mater.* **301**, 171–174 (2006)
- [12] Marx, J., Huang, H., Salih, K. S. M., Thiel, W. R., Schünemann, V.: Spin canting in ferrite nanoparticles. *Hyperfine Inter.* **237**, 41-1 – 41-8 (2016)
- [13] Pandey, B., Litterst, F.J., E.M.Baggio-Saitovitch, E. M.: Preferential spin canting in nanosize zinc ferrite, *J. Magn. Magn. Mater.* **385**, 412-417 (2015)
- [14] Anselmi-Tamburini, U.: Spark Plasma Sintering : in *Encyclopaedia of Materials: Technical Ceramics and Glasses*, Volume **1**, 294-310 (2021).
- [15] Bertaut, E.F.: Etude de la nature des ferrites spinelles. *Comptes Rendus Hebdomadaires des Seances de l'Academie des Sciences* **230**, 213–215 (1950)
- [16] Tanna, A.R., Joshi, H.H.: Computer Aided X-Ray Diffraction Intensity Analysis for Spinel: Hands-On Computing Experience. *World Academy of Science, Engineering and Technology, International Journal of Physical and Mathematical Sciences* **7(3)**, 334–341 (2013)
- [17] Kane, S. N., Verma R., Modak, S. S., Reddy V. R, Mazaleyrat, F. : Structural, Mössbauer and magnetic study of $\text{Co}_{1-x}\text{Zn}_x\text{Fe}_2\text{O}_4$ ($x = 0.0 - 0.56$) nano ferrites. *Hyperfine Interactions* **244**, 3-1 – 3-15 (2023)
- [18] Brand, R.A.: Improving the validity of hyperfine field distributions from magnetic alloys: part I: Unpolarized source. *Nucl. Instrum. Meth.* **B 28**, 398–416 (1987)
- [19] Parmar, C., Verma, R., Modak, S.S., Mazaleyrat, F., Kane, S.N.: Si^{9+} Ion-Irradiation Induced Modification of Structural and Magnetic Properties of Zn-Nanoferrite. *ECS J. Solid State Sci. Technol.* **11**, 053015-1 – 053015-9 (2022)
- [20] Barrera, G., Coisson, M., Celegato, F., Raghuvanshi, S., Mazaleyrat, F., Kane, S.N., Tiberto, P.: Cation distribution effect on static and dynamic magnetic properties of $\text{Co}_{1-x}\text{Zn}_x\text{Fe}_2\text{O}_4$ ferrite powders. *J. Magn. Magn. Mater.* **456**, 372–380 (2018)
- [21] Chen, J. P., Sorensen, C. M., Klabunde, K. J., Hadjipanayis, G. C., Devlin, E., Kostikas, A.: Size-dependent magnetic properties of MnFe_2O_4 fine particles synthesized by coprecipitation. *Phys. Rev.* **B 54**, 9288-9296 (1996)
- [22] Raghuvanshi, S., Tiwari, P., Kane, S.N., Avasthi, D.K., Mazaleyrat, F. , Tatarchuk, T. Mironyuk, I.: Dual control on structure and magnetic properties of Mg ferrite: Role of swift heavy ion irradiation. *J. Magn. Magn. Mater.* **471**, 521-528 (2019).
- [23] Malleth, S., Prabu, D., Srinivas, V.: Thermal stability and magnetic properties of $\text{MgFe}_2\text{O}_4@ \text{ZnO}$ nanoparticles. *AIP Adv.* **7**, 056103–1–056103-8 (2017)

- [24] Srivastava, R. C., Singh, J. P., Agrawal, H. M., Kumar, R., Tripathi, A., Tripathi, R. P., Reddy, V. R., Gupta, A.: ^{57}Fe Mössbauer investigation of nanostructured zinc ferrite irradiated by 100 MeV oxygen beam, *J. Phys.: Conf. Ser.* **217**, 012109-1 – 012109-4 (2010)
- [25] Yusoff, A. H. M., Salimi, M. N., Jamlos, M. F.: Dependence of lattice strain of magnetite nanoparticles on precipitation temperature and pH of solution, *J. Phys.: Conf. Ser.* **908**, 012065-1 - 012065-5 (2017)
- [26] Tiwari, P., Verma, R., Modak, S. S., Reddy, V. R., Mazaleyrat, F., Kane, S. N.: ^{57}Fe Mossbauer study of $\text{CoCr}_x\text{Fe}_{2-x}\text{O}_4$ nano ferrite, *Hyperfine Interactions* **242**, 51–1 – 51–15 (2021)
- [27] Antic, B., Perovic, M., Kremenovic, A., Blanusa, J., Spasojevic, V., Vulic, P., Bessais, L., Bozin, E. S.: An integrated study of thermal treatment effects on the microstructure and magnetic properties of Zn–ferrite nanoparticles *J. Phys.: Cond. Matter* **25**, 086001 -1 - 086001 -13 (2013)
- [28] Raghuvanshi, S., Mazaleyrat, F., Kane, S.N.: $\text{Mg}_{1-x}\text{Zn}_x\text{Fe}_2\text{O}_4$ nanoparticles: Interplay between cation distribution and magnetic properties. *AIP Advances*. **8**, 047804–1–047804-11 (2018)
- [29] Smit, J., Wijn, H.P.J.: Ferrites. Philips Technical Library, Eindhoven (1959)
- [30] Kane, S. N., Satalkar, M.: Correlation between magnetic properties and cationic distribution of $\text{Zn}_{0.85-x}\text{Ni}_x\text{Mg}_{0.05}\text{Cu}_{0.1}\text{Fe}_2\text{O}_4$ nano spinel ferrite: effect of Ni doping, *J. Mater. Sci.* **52**, 3467–3477 (2017)
- [31] Stoner, E.C., Wohlfarth, E.P.: A mechanism of magnetic hysteresis in heterogeneous alloys. *Philos. Trans. R. Soc. London.* **240**, 599–642 (1948)
- [32] Muthuselvam, I. P., Bhowmik, R. N.: Mechanical alloyed Ho^{3+} doping in CoFe_2O_4 spinel ferrite and understanding of magnetic nanodomains. *J. Magn. Magn. Mater.* **322**, 767-776 (2010)
- [33] Satya Murthy, N.S., Natera, M.G., Youssef, S.I., Begum, R.J., Srivastava, C.M.: Yafet-Kittel Angles in Zinc-Nickel Ferrites. *Phys. Rev.* **181**, 969–977 (1969)
- [34] Tiwari P., Verma, R., Modak S. S., Reddy V. R., Kane S. N.: In-field ^{57}Fe Mossbauer study of $\text{Mg}_x\text{Zn}_{1-x}\text{Fe}_2\text{O}_4$ prepared by green synthesis method, *Hyperfine Interactions* **243**, 7–1 – 7–15 (2022)
- [35] Coey, J. M. D.: Noncollinear Spin Arrangement in Ultrafine Ferrimagnetic Crystallites, *Phys. Rev. Lett.* **27**, 1140 – 1142 (1971)
- [36] Kolhatkar, A.G., Jamison, A.C., Litvinov, D., Willson, R.C., Randall Lee, T.: Tuning the Magnetic Properties of Nanoparticles. *Int. J. Mol. Sci.* **14**, 15977–16009 (2013)
- [37] Da Silva, S.W., Nakagomi, F., Silva, M.S., Franco, A., Garg, V.K., Oliveira, A.C., Morais, P.C.: Effect of the Zn content in the structural and magnetic properties of $\text{Zn}_x\text{Mg}_{1-x}\text{Fe}_2\text{O}_4$ mixed ferrites monitored by Raman and Mossbauer spectroscopies. *J. Appl. Phys.* **107**, 09B503–1–09B503–3 (2010)
- [38] Singh, J. P., Payal, R. S., Srivastava, R. C., Agrawal, H. M., Chand, P., Tripathi, A. Tripathi, R. P.: Effect of thermal treatment on the magnetic properties of nanostructured zinc ferrite, *Hyper. Inter.* **217**, 012108-1 012108-4 (2010)
- [39] Kumar, R., Sharma, S. K., Dogra, A., Siva Kumar, V. V., Dolia, S. N., Gupta, A., Knobel, M., Singh, M.: Magnetic Study of Nanocrystalline Ferrites and the Effect of Swift Heavy Ion Irradiation, *Hyperfine Interactions* **160**, 43–156 (2005)
- [40] Van der Kraan, A. M. :Mossbauer Effect Studies of Surface Ions of Ultrafine $\alpha\text{-Fe}_2\text{O}_3$ Particles. *Phys. Stat. Sol. (a)* **18**, 215-226 (1973)
- [41] Mashlan, M., Zboril, R., Machala, L., Vujtek, M., Walla, J., Nomura, K.: Mössbauer Spectroscopy in Study of Thermally Induced Crystallization of Amorphous Fe_2O_3 Nanoparticles, *J. of Metastable Nanocryst. Mater.* **20-21**, 641-647 (2004)
- [42] M. Amir, M, Gungunes, H., Baykal, A., Almessiere. M. A., Sozeri, H., Ercan, I., Sertkol, M., Asiri, S., Manikandan, A.: Effect of Annealing Temperature on Magnetic and Mössbauer Properties of ZnFe_2O_4 Nanoparticles by Sol-gel Approach, *Journal of Supercond. and Novel Magn.* **31**, 3347–3356 (2018)
- [43] Niemantsverdriet, J.W., Van der Kraan, A. M., Delgass, W.N., Vannice M.A.: Small particle effects in Mössbauer spectra of carbon-supported iron catalyst, *J. Phys. Chem.* **89**, 67–72 (1985).
- [44] Kassabova-Zhetcheva, V. D., Pavlova, L. P., Samuneva, B. I., Cherkezova-Zheleva, Z. P., Mitov, I. G., Mikhov, M. T. . Characterization of superparamagnetic $\text{Mg}_x\text{Zn}_{1-x}\text{Fe}_2\text{O}_4$ powders. *Central European Journal of Chemistry* **5(1)**, 107–117 (2007)
- [45] Cherkezova-Zheleva, Z.P, Zaharieva, K. L, Tsvetkov, M.P., Petkova, V. S., Milanova, M. M., Mitov, I. G.: Impact of preparation method and chemical composition on physicochemical and photocatalytic properties of nano-dimensional magnetite-type materials. *American Mineralogist* **100**, 1257–1264 (2015).
- [46] Tsvetkov, M. P., Zaharieva, K. L., Cherkezova-Zheleva, Z. P., Milanova, M. M., Mitov, I. G.: Photocatalytic activity of nanostructure zinc ferrite-type catalysts in degradation of Malachite green under UV-light, *Bulgarian Chem. Comm.* **47(1)**, 354–359 (2015)

Figure captions:

Figure 1 : (a) Schematic of sample synthesis, thermal annealing, (b) Schematic of SPS apparatus, (c) Temperature profile of SPS process.

Figure 2 : XRD patterns of the studied samples. Inset: variation of a_{exp} . For the studied samples, line connecting points are guide to the eye.

Figure 3 : Variation of Oxygen parameter with degree of inversion for the studied samples. Continuous line is linear fit to the data.

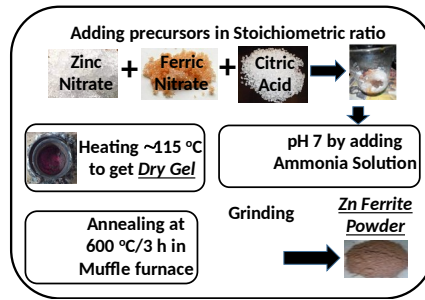
Figure 4 : Variation of bond angles for the studied, DG, ANN, SPS samples. Line connecting points are guide to the eye. Error in the estimation of θ_1 to θ_5 range between $\pm 0.19^\circ$ to $\pm 2.3^\circ$.

Figure 5 : Hysteresis loops of the studied DG, Ann, SPS samples. Inset: variation of $M_{s(exp.)}$ with u . Continuous line is linear fit to the data.

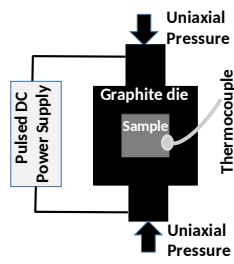
Figure 6 : Variation of: (a) $M_{s(th.)}$, (b) $M_{s(exp.)}$, (c) $M_{s(exp.)}$ with dead layer thickness (t) (Inset: Variation of $M_{s(exp.)}$ with D_{W-H}), (d) Pictorial representation of core (*ordered spin*), shell (*disorder and/or at random spin*) structure for nanoferrite, with applied magnetic field, (e) H_c with K_1 (Inset: Variation of H_c with D_{W-H}), for the studied DG, ANN, SP samples.

Figure 7 : Room temperature Mössbauer spectra of the studied samples. Symbols: experimental data, lines: best fit to the experimental data.

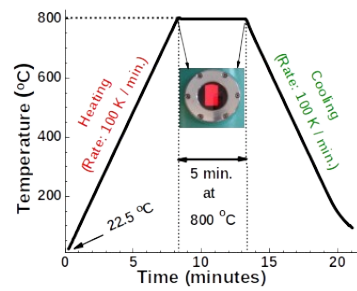
Figure 1 (a to c)



(a)



(b)



(c)

Figure 2

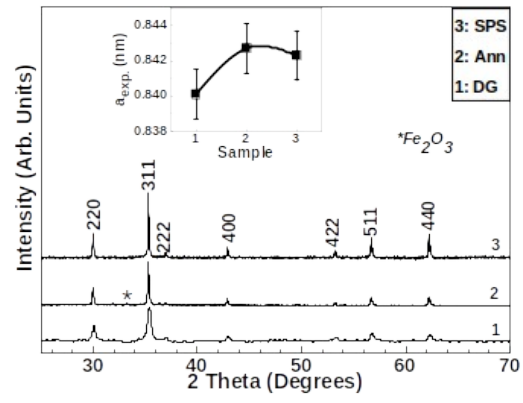


Figure 3

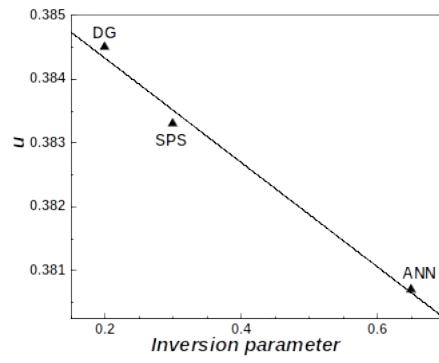


Figure 4

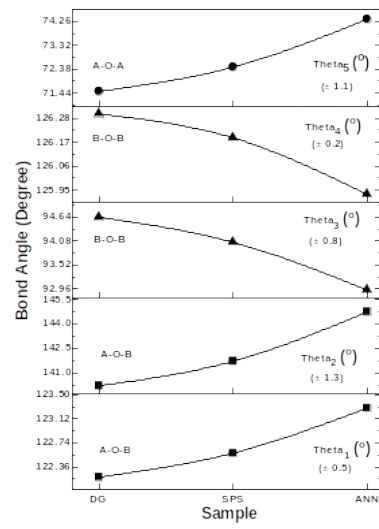


Figure 5

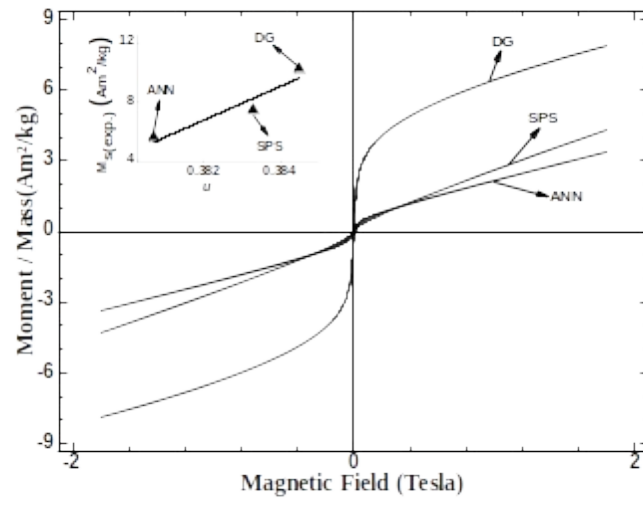


Figure 6 (a to e)

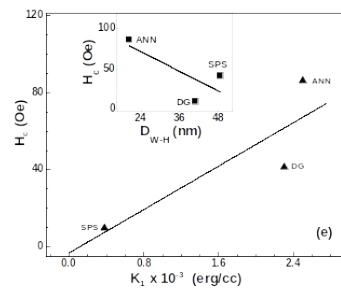
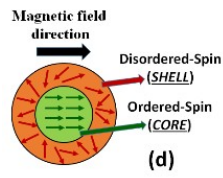
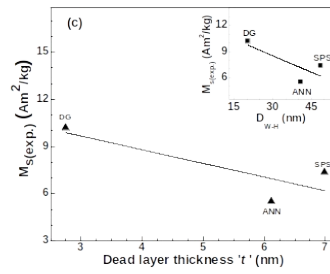
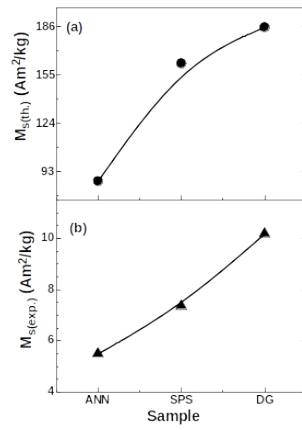


Figure 7

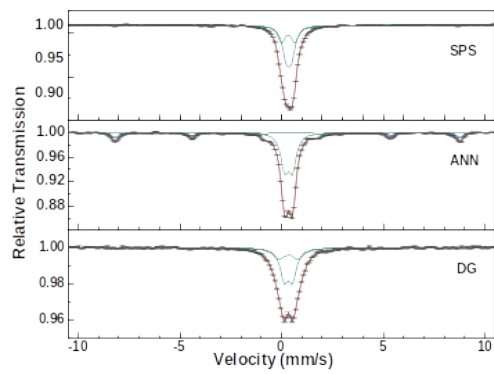


Table 1 Lattice parameter (a_{exp}), Williamson-Hall grain diameter (D_{w-H}), strain (ϵ), dislocation density (ρ_D) for the studied DG, ANN, SPS samples.

Sample	a_{exp} (nm) (± 0.0002)	D_{w-H} (nm) (± 2)	Strain (ϵ) ($\pm 1.4 \times 10^{-5}$)	$\rho_D \times 10^{13}$ (lines/m²) ($\pm 1 \times 10^{13}$)
DG	0.8401	20,3	$- 9.7158 \times 10^{-5}$	8.54
ANN	0.8427	40,9	$- 4.9895 \times 10^{-5}$	2.17
SPS	0.8423	48,6	$- 1.1621 \times 10^{-4}$	4.26

Table 2 Cation distribution (for A, B site), experimental, theoretical lattice parameter (a_{exp} , a_{th}), oxygen positional parameter (u) for studied $ZnFe_2O_4$, and calculated, observed values of intensity ratios I_{220}/I_{440} , I_{400}/I_{422} , I_{220}/I_{400} .

Sample	Cation Distribution (± 0.01)	a_{exp} (nm) (± 0.0002)	a_{th} (nm) (± 0.0002)	u (± 0.0002)	Intensity ratio: (± 0.1)					
					I_{220}/I_{440}		I_{400}/I_{422}		I_{220}/I_{400}	
					Calc.	Obs.	Calc.	Obs.	Calc.	Obs.
DG	$(Zn_{0.80}Fe_{0.20})^A$ $[Zn_{0.20}Fe_{1.80}]^B$	0.8401	0.8440	0.3845	0.972	1.111	1.395	1.291	1.959	2.183
ANN	$(Zn_{0.35}Fe_{0.65})^A$ $[Zn_{0.65}Fe_{1.35}]^B$	0.8427	0.8420	0.3833	0.965	1.220	2.453	2.683	1.793	2.181
SPS	$(Zn_{0.70}Fe_{0.30})^A$ $[Zn_{0.30}Fe_{1.70}]^B$	0.8423	0.8435	0.3807	0.931	1.001	1.602	1.495	1.784	1.867

Table 3 Coercivity (H_c), experimental saturation magnetization (M_s), magnetization at 0 K ($M_s(0\text{ K})$), magneto-crystalline anisotropy (K_1) and Yafet-Kittel angle (α_{y-k}) (obtained from cation distribution), dead layer thickness (t).

Sample	H_c (Oe) (± 3)	$M_{s(\text{exp})}$ (Am ² /kg) (± 2)	$M_{s(\text{th})}$ (Am ² /kg) (± 2)	M_r (Am ² /kg) (± 0.01)	M_r / M_s	$K_1 \times 10^{-3}$ (erg/cc)	α_{y-k} ($^\circ$) (± 2)	t (nm) (± 0.5)
DG	41.17	10.17	185.34	0.69	0.0678	2.307	81.43	2.75
ANN	86.00	5.49	86.88	0.13	0.0242	2.506	60.99	6.12
SPS	9.54	7.35	162.17	0.01	0.0014	0.382	78.56	6.99

Table 4 Fitted Mössbauer parameters (*Width* – Line width, *IS*- Isomer shift, relative to α -Fe, *QS* – quadrupole splitting, B_{HF} – Hyperfine field, area - % Area of the sextet and/or doublet) for the studied DG, ANN, SPS samples.

Sample	Component	Width (mm/s) (± 0.03)	IS (mm/s) (± 0.01)	QS (mm/s) (± 0.03)	B_{HF} (Tesla) (± 0.1)	Area (%) (± 2)
DG	Doublet 1 – SPM , Core	0.47	0.33	0.41	-	53
	Doublet 2 – SPM , Shell	0.72	0.33	0.96	-	47
ANN	Sextet 1 – α -Fe ₂ O ₃ , Shell	0.42	0.38	- 0.20	52.5	21
	Doublet 1 – SPM , Core	0.44	0.34	0.38	-	79
SPS	Doublet 1 – SPM , Core	0.43	0.35	0.25	-	62
	Doublet 2 – SPM , Shell	0.45	0.32	0.65	-	38